

AD-A271 443

ON PAGE

Form Approved
OMB No. 0724-0198



Public
Library
System

This report contains information that is not to be distributed outside the agency or organization to which it is prepared. It is not to be used for advertising or promotional purposes, for advertising or promotional purposes, for advertising or promotional purposes, for advertising or promotional purposes.

1. AGENCY USE ONLY (Leave blank) 2. REPORT DATE: September 30, 1993 3. REPORT TYPE AND DATES COVERED: Reprint

4. TITLE AND SUBTITLE
Measurements and Empirical Model Comparisons of F-region Characteristics and Auroral Oval Boundaries During the Solstitial SUNDIAL Campaign of 1987

5. FUNDING NUMBERS
PE 61102F
PR 2311
TA G5
WU 02

2

6. AUTHOR(S)
E.P. Szuszczewicz, P. Wilkinson, W. Swider, S. Pulnests, M.A. Abdu, E. Roelof, T.Fuller-Rowell, D.S. Evans, T. Bateman, P. Blanchard, G. Gustafson, R. Hanbaba, J. Joselyn, T. Kikkuchi, B. Leitinger, M. Lester, B. Reddy, M. Ruohoniemi, M. Sands, J. Sobral, G.O. Walker, V. Wickwar

7. PERFORMING ORGANIZATION NAME(S) AND ADDRESS(ES)
Phillips Lab/GPS
29 Randolph Road
Hanscom AFB, MA 01731-3010

8. PERFORMING ORGANIZATION REPORT NUMBER
PL-TR-93-2210

DTIC
ELECTE
S A D
OCT 07 1993

9. SPONSORING MONITORING AGENCY NAME(S) AND ADDRESS(ES)

10. SPONSORING MONITORING AGENCY REPORT NUMBER

11. SUPPLEMENTARY NOTES: AUTHOR AFFILIATIONS ON NEXT PAGE
Reprinted from Ann. Geophysicae 11, 601-613 (1993)

12a. DISTRIBUTION AVAILABILITY STATEMENT
Approved for public release; Distribution unlimited

12b. DISTRIBUTION STATEMENT

13. ABSTRACT (Maximum 200 words)
Abstract. We report on the SUNDIAL campaign conducted during the solstitial period May 29-June 7, 1987. For generally quiet conditions a global network of ionosonde data, supported by topside sounder observations of the Intercosmos 1806 satellite, were compared with the International Reference Ionosphere (IRI). The comparisons included F-region peak characteristics, $N_m F_2$ (i.e., $f_o F_2$) and $h_m F_2$, as well as topside height profiles $N_e(z)$. Overall, the IRI specification of $f_o F_2$ was found to be higher than the observations. The difference in the daytime hemispheres was nearly twice that in the night-time hemispheres, with no obvious bias in universal time nor in phenomenological domains (e.g., equatorial anomaly, mid-to-high

latitudes, etc.). With regard to $h_m F_2$ and topside profiles, a small data sample shows relatively good agreement with the IRI. In the topside $N_e(z)$ comparisons there was good qualitative agreement in shape; but there were quantitative differences resulting from differences in $N_m F_2$. To improve IRI specifications at high latitudes comparisons also included Feldstein, DMSP, and NOAA/TIROS auroral oval models and their relative agreements with satellite-borne particle measurements of oval boundaries. The NOAA/TIROS model demonstrates the largest range in dynamic oval boundary responses to magnetic activity.

14. SUBJECT TERMS
F-Region, Auroral oval, Ionospheric modeling, Global ionosphere, Ionospheric parameters

15. NUMBER OF PAGES
13
16. PRICE CODE

17. SECURITY CLASSIFICATION OF REPORT
UNCLASSIFIED

18. SECURITY CLASSIFICATION OF THIS PAGE
UNCLASSIFIED

19. SECURITY CLASSIFICATION OF ABSTRACT
UNCLASSIFIED

20. LIMITATION OF ABSTRACT
SAR

PL-TR-93-2210

Continuation of SF 298, Block 11 Supplementary Notes:

AUTHOR AFFILIATIONS:

E. P. Szuszczewicz¹, P. Wilkinson², W. Swider³, S. Puliners⁴, M. A. Abdu⁵, E. Roelof⁶, T. Fuller-Rowell⁷,
D. S. Evans¹⁰, T. Bateman¹, P. Blanchard¹, G. Gustafsson⁸, R. Hanbaba⁹, J. Joselyn¹⁰, T. Kikuchi¹¹,
R. Lettinger¹², M. Lester¹³, B. Reddy¹⁴, M. Ruohoniemi⁶, M. Sands¹, J. Sobral⁵, G. O. Walker¹⁵, V. Wickwar¹⁶

¹ Laboratory for Atmospheric and Space Sciences, Science Applications International Corporation, 1710 Goodridge Drive, McLean, VA 22102, USA

² DAS, IPS Radio & Space Services, Australia

³ Phillips Lab/GPS, Hanscom Air Force Base, USA

⁴ IZMIRAN, Russia

⁵ INPE, Brazil

⁶ JHU, Applied Physics Laboratory, USA

⁷ CIRES University of Colorado/NOAA Space Environment Laboratory USA

⁸ Uppsala Ionospheric Observatory, Sweden

⁹ CNET, France

¹⁰ NOAA, USA

¹¹ Communications Research Laboratories, Japan

¹² Universität Graz, Austria

¹³ University of Leicester, UK

¹⁴ National Physical Laboratory, India

¹⁵ University of Hong Kong, Hong Kong

¹⁶ Utah State University, USA

Measurements and empirical model comparisons of F-region characteristics and auroral oval boundaries during the solstitial SUNDIAL campaign of 1987

E. P. Szuszczewicz¹, P. Wilkinson², W. Swider³, S. Pulnits⁴, M. A. Abdu⁵, E. Roelof⁶, T. Fuller-Rowell⁷, D. S. Evans¹⁰, T. Bateman¹, P. Blanchard¹, G. Gustafsson⁸, R. Hanbaba⁹, J. Joselyn¹⁰, T. Kikuchi¹¹, R. Leitinger¹², M. Lester¹³, B. Reddy¹⁴, M. Ruohoniemi⁶, M. Sands¹, J. Sobral⁵, G. O. Walker¹⁵, V. Wickwar¹⁶

¹ Laboratory for Atmospheric and Space Sciences, Science Applications International Corporation, 1710 Goodridge Drive, McLean, VA 22102, USA

² DAS, IPS Radio & Space Services, Australia

³ Phillips Lab GPS, Hanscom Air Force Base, USA

⁴ IZMIRAN, Russia

⁵ INPE, Brazil

⁶ JHU, Applied Physics Laboratory, USA

⁷ CIRES University of Colorado, NOAA Space Environment Laboratory USA

⁸ Uppsala Ionospheric Observatory, Sweden

⁹ CNET, France

¹⁰ NOAA, USA

¹¹ Communications Research Laboratories, Japan

¹² Universität Graz, Austria

¹³ University of Leicester, UK

¹⁴ National Physical Laboratory, India

¹⁵ University of Hong Kong, Hong Kong

¹⁶ Utah State University, USA

Received February 27, 1992; revised February 23, 1993; accepted March 4, 1993

93-23623



Abstract. We report on the SUNDIAL campaign conducted during the solstitial period May 29–June 7, 1987. For generally quiet conditions a global network of ionosonde data, supported by topside sounder observations of the Intercosmos 1806 satellite, were compared with the International Reference Ionosphere (IRI). The comparisons included F-region peak characteristics, $N_m F_2$ (i.e., $f_o F_2$) and $h_m F_2$, as well as topside height profiles $N_e(z)$. Overall, the IRI specification of $f_o F_2$ was found to be higher than the observations. The difference in the daytime hemispheres was nearly twice that in the night-time hemispheres, with no obvious bias in universal time nor in phenomenological domains (e.g., equatorial anomaly, mid-to-high latitudes, etc.). With regard to $h_m F_2$ and topside profiles, a small data sample shows relatively good agreement with the IRI. In the topside $N_e(z)$ comparisons there was good qualitative agreement in shape; but there were quantitative differences resulting from differences in $N_m F_2$. To improve IRI specifications at high latitudes comparisons also included Feldstein, DMSP, and NOAA/TIROS auroral oval models and their relative agreements with satellite-borne particle measurements of oval boundaries. The NOAA/TIROS model demonstrates the largest range in dynamic oval boundary responses to magnetic activity.

Correspondence to: E. P. Szuszczewicz

It was also found to be in the best agreement with observations and appears to offer highest promise for a proper high-latitude adjunct to the IRI and an improved empirical specification of ionospheric distributions in auroral zones.

Introduction

Overview

Since October 1984 the SUNDIAL Science Team has conducted a series of coordinated measurement and modelling campaigns to understand better and more accurately predict the global-scale ionosphere in its quiet and disturbed states. The efforts, which include aspects of solar, interplanetary, magnetospheric, and thermospheric physics, focus on understanding the coupling mechanisms as they manifest themselves in global-scale ionospheric responses (Abdu *et al.*, 1988 and 1990; Leitinger *et al.*, 1988; Richmond *et al.*, 1988; Spiro *et al.*, 1988; Szuszczewicz *et al.*, 1988, 1990, and 1992; Biondi *et al.*, 1990; Emery *et al.*, 1990; Fejer *et al.*, 1990; Kikuchi *et al.*, 1990; and Sica *et al.*, 1990). The effort has been covering equinoctial and solstitial periods separated by 9-month intervals with around-the-clock measurements in 8–30 day campaigns that have provided a coordinated international data base throughout the current solar cy-

cle. We report here on the global aspects of the third campaign, conducted during the solstitial period May 29–June 7, 1987. The results focus on the testing of empirical model specifications of the ionosphere and the auroral oval as the zero-order manifestation of magnetospheric inputs; and the measurement/model results reported here define the baseline conditions for other investigations conducted in this campaign [e.g. Walker *et al.*, 1991; Lester *et al.*; Ruohoniemi *et al.*; Abdu *et al.*; Miller *et al.*; Denisenko *et al.* (1993, all in this issue)].

Perspectives on program rationale and approach

The SUNDIAL activities emphasize the comparison of observations with empirical and first-principle models (Szuszczewicz *et al.*, 1988; Schunk and Szuszczewicz, 1988; Spiro *et al.*, 1988; Sica *et al.*, 1990; Wilkinson *et al.*, 1992), in order to provide further tests and validation of the models, improve their accuracy as appropriate, and advance our overall understanding of phenomenologies and associated cause-effect relationships. From an empirical model perspective, the International Reference Ionosphere (IRI) has been the model of choice because it is the most widely used and tested global-scale ionospheric model available to date (Rawer, 1981; Rawer and Ramanamurty, 1985; Schunk and Szuszczewicz, 1988; Wilkinson *et al.*, 1988). Our approach to the IRI and its comparison with our observations is motivated by interest in it as a baseline for time-dependent studies and determination of its integrity as a global-scale specification of conductivity distributions.

Relative to time-dependent studies, one must first ask if a global-scale quiet-time ionospheric condition can be defined, modelled, and tested. This is done more easily on a local or regional basis, but it has yet to be done on a global scale. One can point to averaged conditions (as in the monthly averaged specifications provided by the empirical baseline in the IRI). But by its very definition, the IRI is not a "quiet-time" ionospheric model, and we submit that the scientific community has yet to identify and test a model that specifies the quiet-time global-scale ionospheric electron distribution. This is the point from which studies of dynamics should embark. And we have yet to answer the question as to whether or not the ionosphere is ever in a quiescent state, that is, one in which variations are occurring only with diurnal and semi-diurnal variabilities introduced in first order by solar electromagnetic radiation.

If one can properly specify the quiet-time ionosphere, then one is in the position to specify and delineate global dynamics in ionospheric-thermospheric interactions as manifested in time-dependent chemical, electrical, and momentum coupling processes ... all of which are dependent on the accurate specification of electron density distributions. Studies of momentum coupling and dynamo-driven fields involve the electron density term in the expression for ionospheric conductivity, and there are an ever-increasing number of large-scale numerical models that look to empirical models like the IRI for the specification of global conductivity distributions. If that specifi-

cation is biased, either on a regional or global basis, or if it has diurnal inaccuracies, the large-scale numerical models will unknowingly introduce these biases with an associated distortion in the results.

It is with these perspectives that we approach the IRI. We have developed a global approach that integrates station-by-station results into regional and global representations. In this way we look to uncover trends, biases and inconsistencies, and accordingly point to areas where corrections might be in order. The work reported here still addresses averaged representations, but in a framework that asks to what shorter-period temporal baseline can the monthly-averaged IRI be reasonably applied. Here we make the comparison with a 10-day measurement period and look to biases in global perspectives, universal time, and diurnal characterization. This is done with a focus on the critical frequency (i.e., the density of the F-region peak) as measured on the bottom-side by a global distribution of ionosondes.

Our bottom-side model-measurement comparisons are complemented by model-measurement comparisons using the Intercosmos 1806 topside sounder in regions less accessible to its ground-based counterparts. This is done as an initial effort to test IRI specifications of topside profiles, to expand the database, and to establish a cross check on any trends that might be observed in the bottomside network.

Finally, we address one of the most fundamental deficiencies in the IRI, its representation of the high-latitude ionosphere, particularly as it is affected by particle precipitation in the auroral oval and by variabilities in the position of the oval in periods of geomagnetic storms. Three empirical models of the auroral oval (the Feldstein, DMSP and NOAA/TIROS models) are reviewed and tested against a data base developed during the SUNDIAL period. This comparison establishes a quantitative comparison of the individual model specifications of auroral oval boundaries (as a function of geomagnetic activity) and provides the initial stage for improving the IRI specification of the high-latitude ionosphere.

Our overall results are cast in global-scale perspectives that include not only the results developed during the 1987 solstitial campaign but involve comparisons with the equinoctial study of 1986. The objective is the identification of trends, biases, and regions for improvement, in a way that represents stepwise progress toward an accurate specification of the global-scale ionosphere in its quiescent and dynamic states. The 1986 and 1987 results represent the solar-minimum ionospheric baseline for the remainder of the SUNDIAL campaigns conducted throughout the ascending and solar-maximum phases of the current solar cycle.

Global F-region measurements and model comparisons

Prevailing solar-terrestrial conditions during the 1987 campaign

Unlike the first two SUNDIAL campaigns, the May 29–June 7, 1987 campaign was solstitial (as opposed to

SUNDIAL CAMPAIGN1-10 JUNE 1987
DATA/MODEL COMPARISONS: ALL STATIONS ALL TIMES

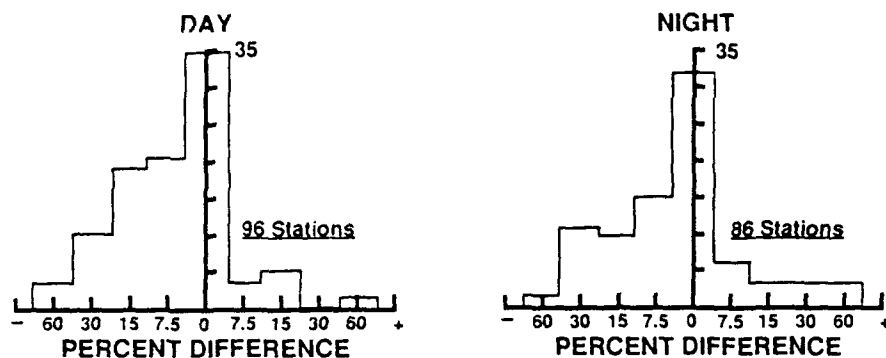


Fig. 1. Distributions showing the number of ionosonde stations (the ordinate) with measurements that were larger or smaller (expressed as percent difference along the abscissa) than those specified by the IRI for the campaign period of June 1987. The results were integrated over all times and separated only according to the day-

time or night-time hemispheres. Percent differences at 0, 7.5, 15, 30, and 60 correspond to the data/model comparison bins used in Figs. 3 and 4 of $\pm 5\%$, 5–10%, 10–20%, 20–40%, and $>40\%$, respectively. The total number of stations included in each histogram distribution is specified in the panels

equinoctial). It occurred during the early months of solar cycle 22, involved no major storm activity, and for most practical aspects was geomagnetically quiet. There were no significant solar flares, the Covington index for the 10.7 cm flux was low (approximately 75 solar flux units), and the solar wind characteristics were dominated by steady, low-speed streams with velocities typically between 300 and 400 km s⁻¹, and an excursion to speeds near 500 km s⁻¹ on June 2nd. The geomagnetic field was also quiet, with some minor activity on May 29 and June 6 when the 3-h planetary K_p indices approached values near 5. Otherwise, K_p levels varied between 0⁺ and 2⁺ throughout the other campaign days.

Bottomside sounder comparisons

We focus here on the IRI and on ionosonde observations of peak F₂-region electron densities at 0, 6, 12, and 18 UT covering the June 1–10 period of 1987. (The ionosonde data base was extended beyond the planned May 29 to June 7 period to provide an improved justification for comparison with the monthly-averaged ionospheric specification of the IRI defined for that month.) The results of nearly 50 stations are presented in two formats. The first, depicted in Figs. 1 and 2, integrates the model-measurement comparisons to look for global trends identifiable with diurnal (day/night) and universal time (UT=0, 6, 12, and 18) variabilities. The second, presented in Figs. 3 and 4, provides a world-wide view of individual station results with a perspective on potential regional and morphological influences.

In the format of a probability distribution of station observations as a function of percent differences between the measurements and the model, Fig. 1 integrates all the results without regard to region or universal time, but focuses on potential differences in day/night results. That figure shows that the observations are skewed in the direction of values less than those of the IRI. Specifically,

the comparison shows that the data differed from the IRI in the daytime hemisphere by an amount nearly twice the difference in the night-time hemisphere (-7.13% vs -4.1% , respectively). On an overall average, therefore, the IRI overpredicted the values of $f_0 F_2$ by 5.6% (corresponding to an average overestimate of 11.2% in N_e at the F-region peak). While these averaged values are not of alarming proportions, the data show a substantial number of station with the IRI specifications for $f_0 F_2$ being 15–30% higher than the actual measurements. In terms of N_e , this corresponds to a 32–69% overspecification by the IRI.

Figure 2 partitions the day/night comparisons into the UT=0, 6, 12, and 18 periods to look for trends in the model-measurement comparison with biases in universal time. That figure maintains the general trend of a negative bias in the observations when compared with the IRI, without any obvious dependence on universal time. Noticeable departures from this trend might be attributed to the UT=0 (daytime) and UT=6 (night-time) cases. The former case maintains the general trend (i.e., a negative bias in the data distribution), but is strongly skewed with the most probable value being -15% . By comparison, the UT=6 (night-time) case shows a uniform distribution, but here the station statistics were small.

We investigate the UT=0 and 6 cases more fully and explore the possibility for regional biases in the global presentations in Figs. 3 and 4 where the individual station results are plotted against a background of “predicted” $f_0 F_2$ [$= 8.9(10^3) \sqrt{NmF_2} [\text{cm}^{-3}]$] contours from the IRI for the month of June under near-solar-minimum conditions (SSN=30). The symbols (triangles, circles, and squares) locate the stations and quantify the level of agreement/disagreement between the observations and the model specifications. (The quantitative significance of the symbols is fully defined in the caption of Fig. 3.) Included in each plot is a Q=4 Feldstein oval (Feldstein, 1963; Holzworth and Meng, 1975) and vertical bars at the 6 am and 6 pm LT meridians. (The Q=4 condition is

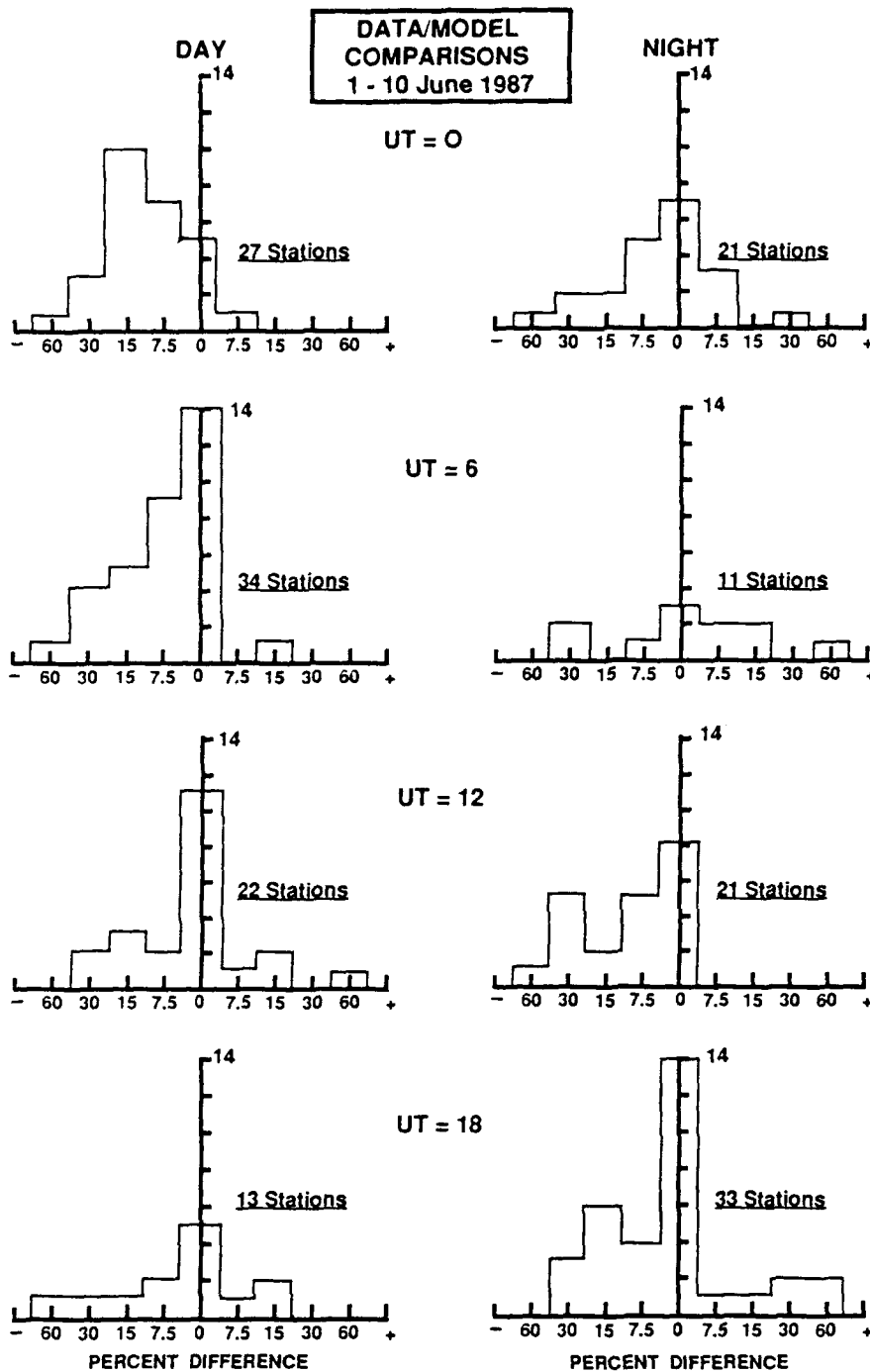


Fig. 2. Same as Fig. 1 except the data is further partitioned to reflect the distributions at UT=0, 6, 12 and 18 h

geomagnetically equivalent to $K_p=2$, an approximate average for the period under study.)

The daytime hemisphere data at UT=0 (Fig. 3) is dominated by stations in the Japan-Australian meridian, stretching from sites inside the southern auroral oval to northern latitudes in excess of 60° geographic. The temporal period is primarily mid-morning, with high-, mid- and equatorial coverage. The data-model presentation shows that the differences are everywhere consistent. Virtually without exception in this meridional mid-morning zone the IRI predicts values of $f_0 F_2$ that are greater than the observations, and this is without bias in morphologi-

cal domain. These same conclusions apply during afternoon hours, as can be seen in Fig. 4.

Further inspection of Fig. 4 shows that station statistics are very good (poor) in the daytime (night-time) hemisphere. In the daytime hemisphere, where the trend has been more negatively biased than in its night-time counterpart (for all UT), the only departures from that trend is at high northern latitudes within Europe and the former Soviet Union. It is these stations that drive the most probable value in the UT=6 (daytime) distribution to 0%.

The dominant feature in Figs. 1-4 (and in UT=12 and 18 comparisons of individual station results not pre-

nal cycle, could provide unjustified perspectives on the model capabilities as a result of undersampled testing. We provide some insight into this perspective using full diurnal characteristics of $f_0 F_2$ values for Cachoeira Paulista (31° E long, -22.7° lat, -12.4° mlat) in Brazil and for Canberra (149° E long, -35.3° lat, -43.7° mlat) in Australia. These data (in Figs. 5 and 6, respectively) have been selected since they represent mid-to-equatorial sites separated by almost 180° in longitude, and one of them (Canberra) is included in the Intercosmos 1806 topside comparisons presented in the next section.

Figures 5 and 6 show the values specified by the IRI for the month of June for a sunspot number equal to 30. The figures also include two data plots. One reflects the value of $f_0 F_2$ averaged over the first 10 days of June (as done in the development of the global comparisons in Fig. 3 and 4) and the second reflects the averaged values for data collected throughout the entire month of June.

The 10-day averages are similar to the 30-day averages. This is certainly the case in a comparison of the qualitative features of the diurnal behaviors in both data sets and between the data and the specifications of the IRI. On a quantitative basis, Canberra's 10-day data tends to be about 15% lower than the 30-day data during the night-time period but in near perfect agreement in the daytime. Had the 30-day data been the baseline for the comparisons in Figs. 1 and 2, the results would have been the same at Canberra for daytime measurements but shifted by a 5%–10% difference in the positive direction at night.

The plots for Cachoeira Paulista show very good agreement between the 10- and 30-day data sets, with some differences in the period between 12 and 20 UT. Both data sets are in very good agreement with the pre-sunrise minimum but the values differ markedly with the sunset minimum of the IRI. In all cases, the 10- and 30-day data sets show values less than those of the IRI. The data sets and the IRI also reflect the influences of the equatorial anomaly in the late afternoon (UT \approx 19 hr). The most significant difference between the model and the observations involves the absolute values of $f_0 F_2$, within the 0 and 16 UT time frames. These differences are approximately 40% and 30%, respectively.

Topside profiles

The accuracy of the IRI was further investigated by including comparisons of IRI topside ionospheric density profiles with the sounder observations of the Intercosmos 1806 satellite. Those results are shown in Fig. 7, together with F-region heights $h_m F_2$ and peak densities $N_m F_2$ determined by ground-based ionosondes at several sites co-registered with the satellite soundings. Figure 7 corresponds to data on June 4 and 5 in the Australian-Japan sector near 150° E longitude, at an average time of UT = 4.30 h (LT = 13.8 h):

Relative to a comparison between the topside sounder and IRI profiles we offer the following comments: 1. the satellite data represent mid-to-low latitude domains near local noon; 2. qualitatively, the shapes of the $N_e(z)$ pro-

files are similar; 3. the observed sounder densities are generally less than those in the IRI (in agreement with previously discussed results); and 4. the agreement in the topside profiles would be improved if the peak densities in the IRI were reduced (as suggested by both the topside and bottomside sounder findings).

Ground ionosonde stations near subsatellite positions are identified in the panels and the plots include the associated ground-station measurements of the monthly median and upper/lower decile values for $N_m F_2$ and $h_m F_2$ (depicted as +) as well as their ($N_m F_2$, $h_m F_2$) instantaneous point values at UT = 4 h on June 4 (depicted as ●). The topside and bottomside sounder results are seen to be in good agreement. There are several points worth noting about the results in Fig. 7:

First, as a monthly averaged specification the IRI is more properly compared with the monthly averaged bottomside sounder determinations of $N_m F_2$ and $h_m F_2$ (the "crosshairs" in panels A-E). For all cases in Fig. 7 with co-registered ground-station data, the peak electron densities agree well with the IRI and are always within the decile range of the observations. The tendency, however, is for the measured monthly median values of $N_m F_2$ to be less than those specified by the IRI, consistent with the results in Figs. 1 and 2. The peak height values (monthly median) are also systematically lower than the IRI (apart from Hobart) but agreement is achieved within the decile.

Second, the IRI has often been criticized for its topside profile specification and its associated representation of the total electron content (see, e.g. Bilitza, 1985). Our small data sample suggests that the problem with the IRI is not so much the shape of the topside profile but rather its reference point ($N_m F_2$, $h_m F_2$). With this being a variable that is locally adjustable in the IRI, the model agreement with observed topside profiles can be very good.

Empirical auroral oval models and observations

Potentially more serious deficiencies in the IRI exist than the inaccuracies in $N_m F_2$ and $h_m F_2$. These deficiencies have been discussed in earlier works (Szuszczewicz *et al.*, 1988; Schunk and Szuszczewicz, 1988) where it has been pointed out that areas requiring attention include high latitudes (with emphasis on domains involving energetic particle precipitation). We have given some attention to the high latitude deficiency and executed a comparison of empirical oval models that offer the possibility of a meaningful adjunct to the IRI. Here we discuss and compare: 1. the Feldstein oval based on photographic data; 2. the DMSP model based on "in situ" particle data collected in the Defense Meteorological Satellite Program (DMSP); and 3. the NOAA/TIROS model based on particle flux and energy measurements conducted in a series of NOAA environmental satellite missions.

Feldstein oval

The Feldstein oval model (Feldstein, 1963) is based on photographic data of auroral oval morphology in the

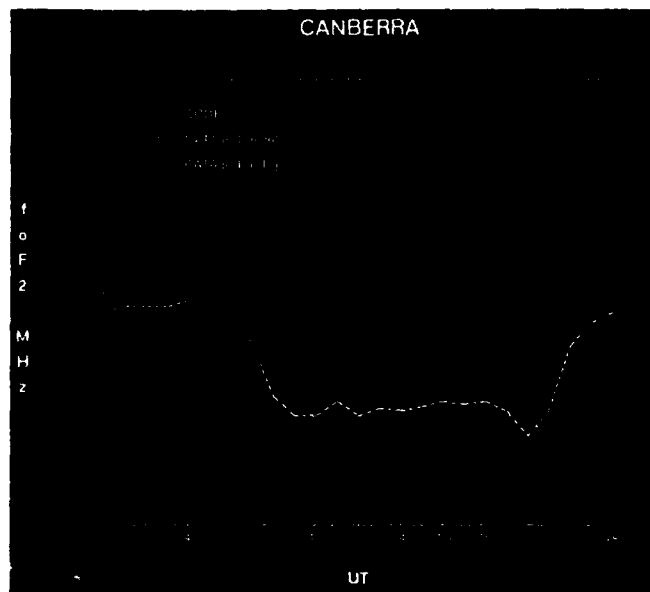


Fig. 5. Diurnal variations of $f_o F_2$ at Canberra, Australia (-35.32° lat., 149° E. Long., -43.68° dipole lat.). The red curve represents the "predictions" of the IRI, while the green and yellow curves are the median ionosonde observations for June 1–10 and June 1–30, respectively

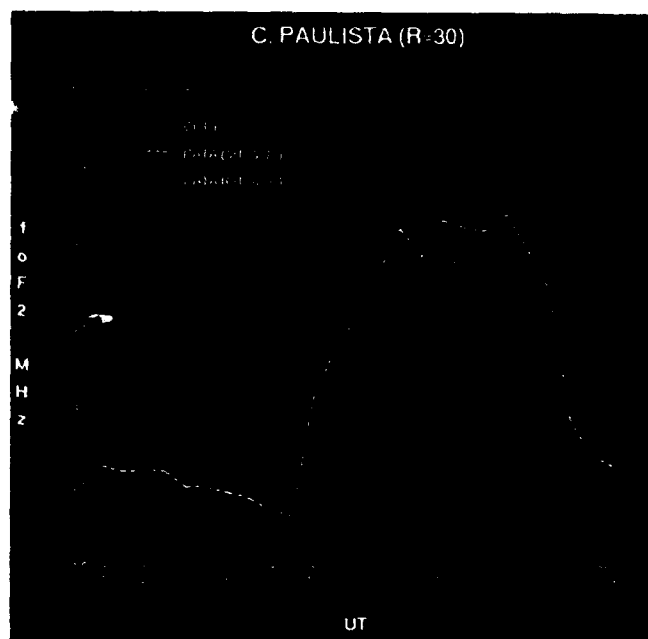


Fig. 6. Diurnal variations of $f_o F_2$ at Cachoeira Paulista, Brazil (-22.70° lat., 46.0° E. long., -12.40° dipole lat.). The red curve represents the "predictions" of the IRI, while the green and yellow curves are the median ionosonde observations for June 1–10 and June 1–30, respectively

northern and southern hemispheres collected during the International Geophysical Year (from November 1957 through February 1958 in the northern hemisphere and from May 1958 through August 1958 in the southern hemisphere). The oval boundaries are represented by a Fourier series (spherical harmonics) of order 4, with the constants in the series determined by a least-squares analysis to minimize errors between data and the fitting function (Holzworth and Meng, 1975).

DMSP oval

Data used to develop the DMSP model (Hardy *et al.*, 1987) were acquired by three satellites, F2 and F4 from the Defense Meteorological Satellite Program (DMSP), and P78-1 from the Space Test Program. F4 had a circular sun-synchronous orbit with an 840 km altitude and an inclination of 97.4° in the 1000–2200 h meridian. F2, also at 840 km circular, was to be sun-synchronous in the dawn-dusk meridian but its orbit precessed toward the 0800–2000 h meridian over its 2.5-year lifetime. The P78-1 satellite was in a 600 km circular sun-synchronous orbit in the noon-midnight meridian.

Data were available from September 1977–February 1980 using F2, from April 1979–August 1980 using F4, and from February 1979–January 1980 using P78-1. The F2 satellite recorded data from 17 000 northern and southern hemisphere passes, while 10 000 passes were recorded by the F4 satellite. There were 1800 hemispheric passes provided by the P78-1 satellite. However, only spectra with the detector look-direction pointed toward

the local zenith were used. (The look-direction of the F2 and F4 detectors always pointed toward the local zenith.)

One complete energy spectrum (50 eV to 20 keV) was produced every second from the F2 and F4 detectors, while four energy spectra were produced every second from the P78-1 detector. To provide an even distribution of data over the seasons of the year and to provide sufficient coverage at high activity, 15 months were chosen from the F2 and F4 data and 12 months of data were used from the P78-1 satellite.

Using all the spectra that fell within a given MLT and CGMLAT zone, the average and standard deviations of the differential number flux for each of the 16 detector energy channels were calculated. The final result was an average spectrum for each zone at a given level of activity. These average spectra were fitted using an Epstein transition function to provide a representation of the asymmetric shape of the auroral oval. Because the coefficients used in the mathematical fitting procedure were slowly-varying functions of magnetic local time, they were determined by expanding their MLT dependence in a Fourier series of order 6 (thereby reducing the number of coefficients needed).

In performing a least-squares analysis of the fitting function to the data, only values above a specified minimum were used. This was to exclude the values below the auroral zone and in the polar cap where the four quantities (i.e., integral energy flux, integral number flux, Hall and Pedersen conductivities) are roughly constant and small, or zero. For the integral energy flux and integral number flux, the minimum value was 10^6 keV $(\text{cm}^2 \text{ s sr})^{-1}$ and 10^6 el $(\text{cm}^2 \text{ s sr})^{-1}$, respectively, to the equatorward

COSMOS - 1809 Topside Sounder and SUNDIAL/IRI Comparisons

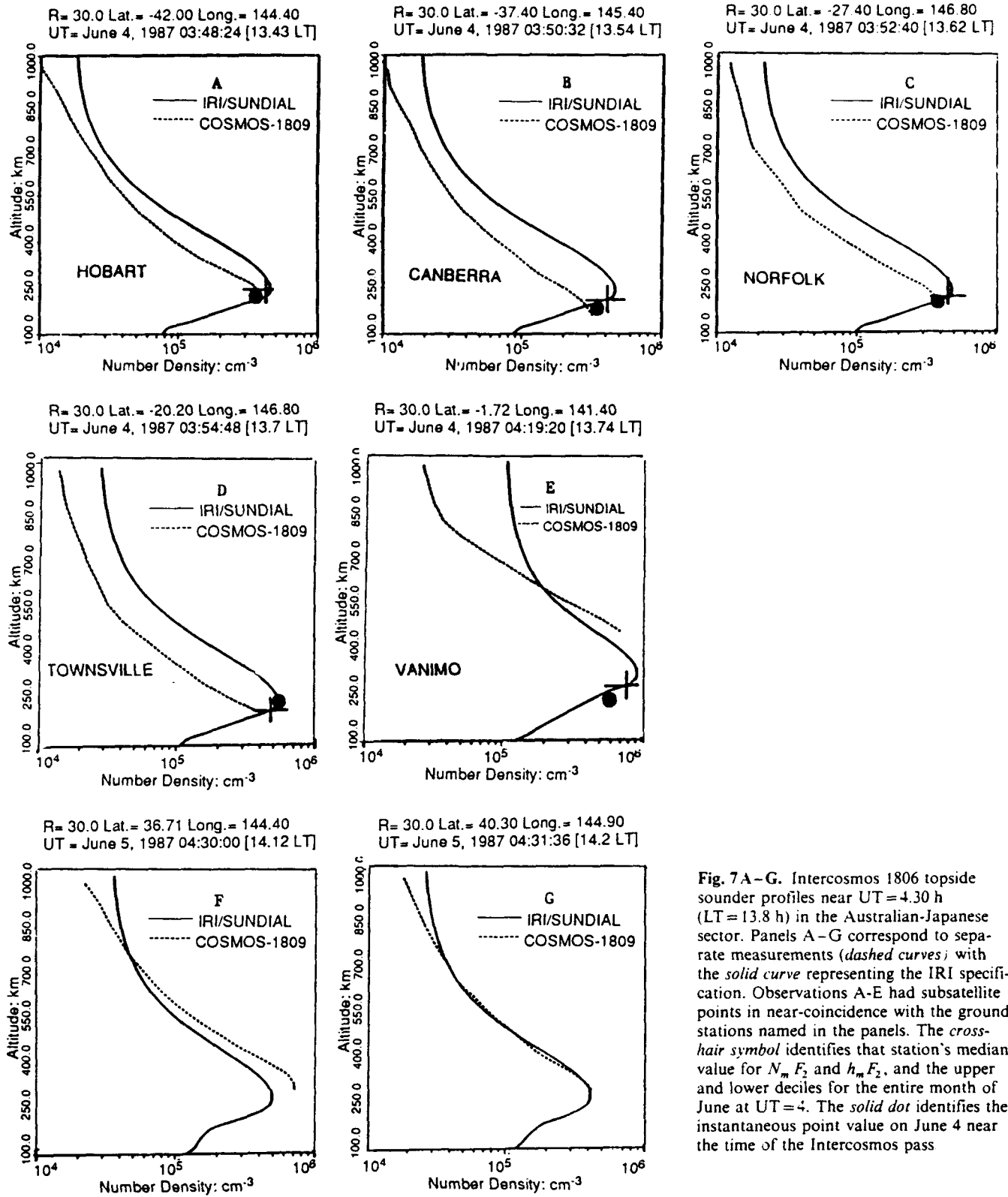


Fig. 7 A-G. Intercosmos 1806 topside sounder profiles near UT = 4.30 h (LT = 13.8 h) in the Australian-Japanese sector. Panels A-G correspond to separate measurements (*dashed curves*) with the *solid curve* representing the IRI specification. Observations A-E had subsatellite points in near-coincidence with the ground stations named in the panels. The *cross-hair symbol* identifies that station's median value for $N_m F_2$ and $h_m F_2$, and the upper and lower deciles for the entire month of June at UT = 4. The *solid dot* identifies the instantaneous point value on June 4 near the time of the Intercosmos pass

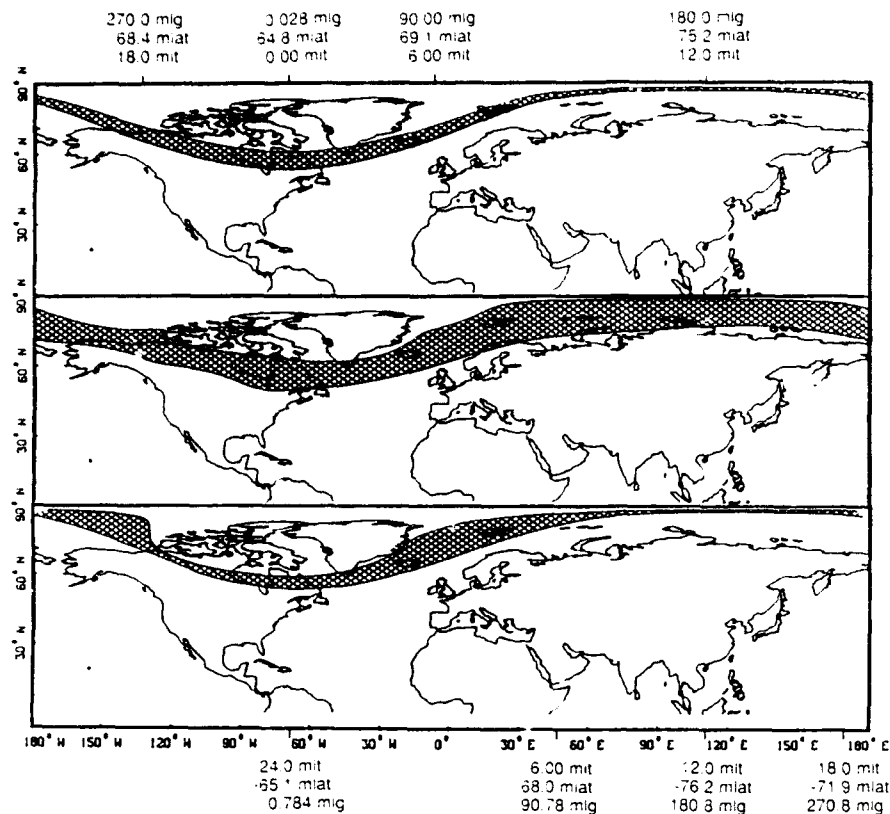


Fig. 8. Northern hemisphere auroral oval model comparisons at UT = 4.7 for equivalent activity indices. The top panel shows the Feldstein oval with $Q=3$. The middle panel shows the DMSP oval with $K_p=1$, and the bottom panel shows the NOAA/TIROS oval with $AI=3$.

side of the maximum value and 10^7 to the poleward side. Likewise, for the height-integrated Hall and Pedersen conductivities, the minimum value was 1 mho for both the equatorward and poleward boundaries (Hardy *et al.*, 1987).

The minimum height-integrated Hall conductivity of 1 mho was chosen to represent the oval boundary in our comparison studies since Hall conductivity involves both number and energy flux, and uses data from the instrument channels corresponding to energies higher than about 500 eV (Robinson *et al.*, 1987). This assures representation of more energetic particle effects and minimizes the contribution of "drizzle" particle energies toward the polar cap.

NOAA/TIROS oval

The NOAA/TIROS oval model (Evans *et al.*, 1988; Fuller-Rowell and Evans, 1987) is based on data from the NOAA/TIROS weather satellites carrying particle detectors capable of measuring energies in the range 300 eV–20 MeV. Data were obtained over an 8-year period from 1978 to 1988 consisting of spectra from more than 60 000 passes across the polar regions. The satellites were in sun-synchronous orbits at an altitude of 850 km.

From a given polar pass, the total precipitating particle power input was estimated and assigned an activity index. All passes within a given activity index (AI) were averaged in magnetic latitude and magnetic local time bins. The MLT was binned in 8-min intervals and MLAT was divided into 1° intervals. Activity indices ranged from

1 (very quiet) to 10 (active). (More information on the binning method and data gathering is provided in Foster *et al.*, 1986).

The program developed within the SUNDIAL investigation to determine the NOAA/TIROS oval boundaries searched through the data for entries with energy fluxes greater than $0.25 \text{ ergs (cm}^2 \text{ s)}^{-1}$. The energy flux of $0.25 \text{ ergs (cm}^2 \text{ s)}^{-1}$ was the suggested definition of the aurora oval edge (D. Evans, private communication). By interpolating between the two entries, the magnetic latitude and magnetic local time of the oval boundaries were determined for a given activity index. Because the boundary locations exhibited a "spiky" structure when displayed on a magnetic latitude/local time plot, the oval edge data were smoothed using a Fast Fourier Transform (FFT). This curve is used to define the auroral oval.

Intercomparison of the three models

Each of the three empirical oval models uses a different index to specify the overall geomagnetic activity (and thus the boundary of the oval). These indices (Q , K_p , and AI for the Feldstein, DMSP and NOAA/TIROS models, respectively) are all traceable to magnetic field fluctuations and are interrelated in a linear fashion as represented in Table 1.

To illustrate and compare the global latitudinal coverage of these oval prescriptions, Fig. 8 presents the oval boundaries produced by each model (i.e., Feldstein, DMSP, and NOAA/TIROS, respectively) for a universal time (UT) of 4.7 hr (corresponding to a midnight magnet-

Table 1. Relationships between the activity indices used in the Feldstein, DMSP, and NOAA/TIROS auroral oval models

K_p	0	1 ⁻ 1 ⁺ 1*	2 ⁻ 2 ^o 2*	3 ⁻ 3 ^o 3*	4 ⁻ 4 ^o 4*	5 ⁻ 5 ^o 5*	6 ⁻ 6 ^o 6*	>6*
K_p^*	0	1	2	3	4	5	6	6
Q^{**}	0, 1, 2	3	4	5	6	7	8	8
AI ^{***}		1 2 3	4 5	6 7	8	9	10	

* K_p specification used by Hardy *et al.* (1985)

** Used relation $K_p = 0.33 Q$ for $Q < 3$, and $K_p = Q - 2$ for $Q \geq 3$

*** Foster *et al.* (1986)

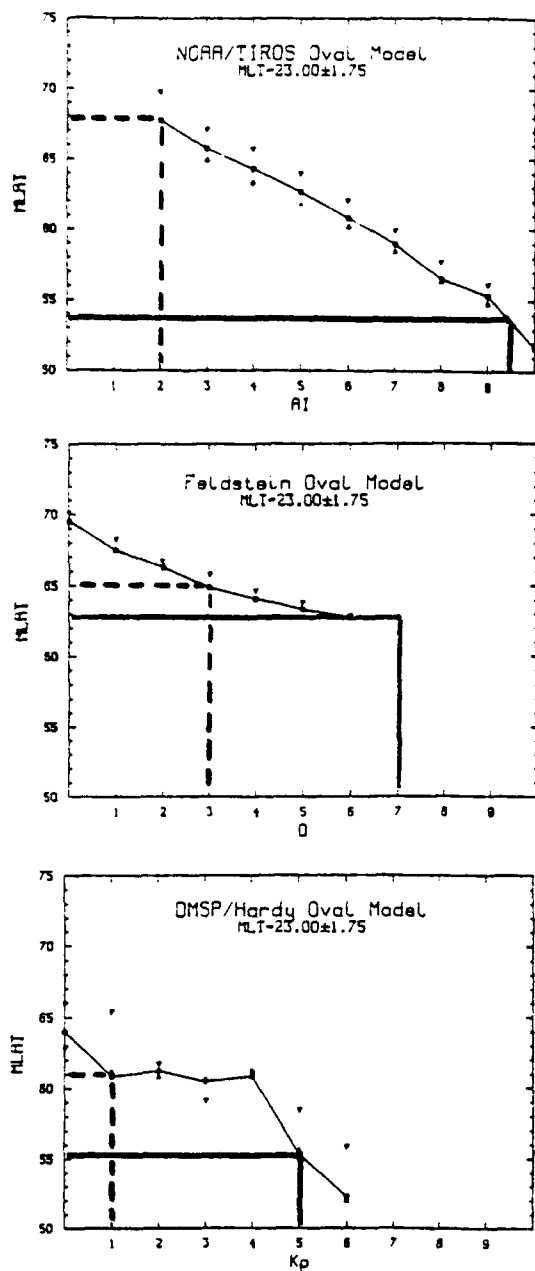


Fig. 9. MLAT of the equatorward boundary for a given level of magnetic activity as defined in the NOAA/TIROS (*top panel*), the Feldstein (*middle panel*), and the DMSP (*bottom panel*) models, respectively. The **bold solid** (red) and **dashed** (blue) lines identify the extrema in magnetic activity during the May 29–June 7, 1987 period. The **triangles** identify the upper and lower deciles of the MLAT values in the 2300 ± 1.75 h time domain

ic local time near the 0° magnetic longitude meridian) and activity levels corresponding to Q , K_p , and AI equal to 3, 1, and 3, respectively. These activity levels represent equivalent quiet conditions within the framework of activity indices defined in each model.

The results in Fig. 8 are characteristic of our comparisons of the oval models for other levels of magnetic activity. These characteristics fall into three general categories: 1) shape, 2) oval thickness, and 3) equatorward extent for comparable levels of magnetic activity. Relative to shape, the Feldstein oval always represents a simple displaced-annular-ring; while DMSP and the NOAA/TIROS results display a more complicated shape reflecting the nature of the model fit to the satellite data. DMSP and NOAA/TIROS ovals are also thicker than the Feldstein approach and they tend to manifest a greater equatorward penetration of the oval for comparable activity levels. The DMSP oval tends to reflect the most complicated geometry and the most equatorward boundary.

The dynamic range of the three models and their "responsiveness" to magnetic activity are presented in Fig. 9. The figure shows the equatorward boundary "predicted" by each of the empirical models at 2300 ± 1.75 h MLT. The solid and dashed lines reflect the range in the activity indices during the SUNDIAL interval, along with associated positions of the equatorward boundaries at the extrema of observed activity. Several comments are in order: 1) the NOAA/TIROS model generally predicts a more linear behaviour and a greater dynamic range than the other two models; 2) the smallest latitudinal range occurs in the Feldstein model; and 3) the DMSP model manifests some "anomalous" characteristics as a result of the mathematical fitting function utilized in its empirical formulation.

Comparison of oval models with observations

To test the relative accuracy of these oval prescriptions and illustrate the dynamics of the oval during the 1987 campaign period, we focus on the equatorward boundary of each of these models near local magnetic midnight and compare the results with DMSP satellite measurements of energetic particle fluxes during the May 29 to June 7, 1987 period.

The satellite data were based upon 15-s averages, with a complete energy spectrum determined every second, and the boundaries were identified as those points at which the count rate for 1–10 keV electrons exceeded the

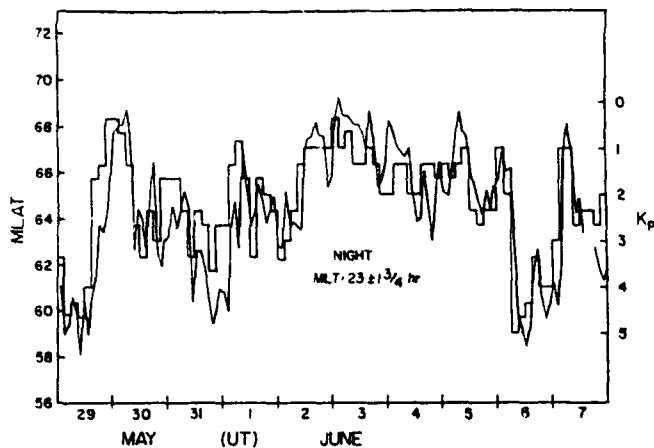


Fig. 10. Composite representation of K_p values and measured equatorward boundaries of the auroral oval by particle fluxes on the DMSP satellite during the period May 29–June 7, 1987. The data were binned in the time frame 23 ± 1.75 h MLT



Fig. 11. Comparison of the NOAA/TIROS model with DMSP particle data observations of the equatorward boundary of the auroral oval during the SUNDIAL-87 campaign

background count rate by at least a factor of 10. With this definition, the measured equatorward boundary of the oval at 2300 ± 1.75 h is plotted in Fig. 10 along with the prevailing K_p values during the SUNDIAL period. Inspection of that figure shows that the boundary dynamics conform to intuition, moving more equatorward (poleward) with increasing (decreasing) values of K_p .

In comparing the data with each of the three models, we found the NOAA/TIROS oval agreed best with the observations (see Fig. 11). Qualitatively, the model and the measurements show very good correlation in tracking the positive and negative excursions in the values of the K_p activity index. Quantitatively, the comparison reveals typical differences ranging from 1° – 2° in MLAT and never worse than 5° . The biggest "errors" occur during dynamic transitions as on May 29 and 30 and again on June 6.

While the comparison presented here is by no means exhaustive, it reflects the merits of the NOAA/TIROS oval model. Like the DMSP model, it is based on "in situ" energetic particle data but manifests better mathematical performance and includes an empirical specification for the high latitude convection patterns that are consistent with the ovals and tunable to prevailing geomagnetic conditions (see e.g., Foster *et al.*, 1986). It is also updatable from an on-line NOAA/TIROS data source; and with the convection pattern capability, it lends itself to adaptive modeling techniques and a broader spectrum of utilities when coupled with an ionospheric model such as the IRI.

Comments, conclusions and future directions

Our results have focused on continued testing of IRI model specifications of the global-scale F-region ionosphere with complementary efforts on the potential for an auroral oval adjunct to include the zero-order manifestations of magnetospheric inputs. Our approach to the IRI and its comparison with our observations of $N_m F_2$, $h_m F_2$ and topside profiles has been motivated by interest in it as a baseline for time-dependent studies and determination of its integrity as a global-scale specification of conductivity distributions. Overall, we continue to conclude that the IRI is the best global-scale empirical ionospheric model available to date. We note however, that the 1987 solstitial results reported here as well as the 1986 equinoctial SUNDIAL results showed that the IRI specifications of $f_o F_2$ were consistently higher than the observations.

We also note that the empirical modelling of F-region characteristics through $N_m F_2$ and $h_m F_2$ represents the most simple component in specifying the overall ionospheric morphology. This has dominated our approach to date largely because these parameters are generally a routine data product in ionosonde observations. The more difficult problem is faced at F_1 - and E-region domains, where the height profile information can be hidden by intense underlying layers and where the density distributions can depart in major ways from the classical laminar descriptions of the E- and F_1 -domains. This is particularly true in the presence of intermediate, transitional, descending, or otherwise sporadic layers (Wilkinson *et al.*, 1992). These layers are produced by thermospheric winds, electric fields, and ion composition effects, and they can play an important role in modifications of lower ionospheric conductivities and dynamo-driven fields. It is in this lower ionospheric-thermospheric domain that major advances in empirical modeling are important. It is therefore necessary that the diurnal, seasonal, and solar-cycle variability of these intermediate and sporadic layers be properly defined, not only to upgrade empirical model specifications but to provide an empirical baseline upon which to test, validate, and improve first-principle models. This type of effort has been started recently in the SUNDIAL program, with some advances made in the diagnostics and analysis of these layers through careful treatment of ionogram data coupled with first-principles modeling support (Wilkinson *et al.*, 1992). This effort will

continue on a global scale, with the intention being an improved empirical specification of this lower ionospheric domain.

This lower region and its associated plasma structures are also modified in important ways by energetic particle precipitation at high latitudes. This has long been a criticism of the IRI. Our initial efforts to mitigate this problem has been to explore the potential to include an empirical specification of the position and dynamics of the auroral oval boundaries. At a minimum, this will help identify the location and movement of the oval (at least as made possible by the averaging processes built into the models) and facilitate the identification of cause-effect terms for related aspect of global-scale ionospheric dynamics. Future efforts suggest that associated enhancements in the ionospheric densities should also be incorporated into the IRI in order to reflect ionization processes resulting from the precipitating energetic particles. The appropriate strategy here is not clear, due in part to the complex nature of the spatial and temporal variability of particle precipitation patterns. Future activities should investigate this aspect of the empirical modelling problem, with the intention primarily focused on the use of such obvious inputs as the energy and density fluxes specified in the DMSP and NOAA/TIROS models. Referring now to our comparisons of these two models, as well as the much-used Feldstein oval, we note that our tendency is to favor the approach of the NOAA/TIROS results, partly because of its (apparently proper) dynamic range, its inclusion of high-latitude convection field patterns (derived self-consistently with the oval boundaries and cross polar-cap potentials), and the model agreement with the observations conducted during the June 1987 campaign.

Primary deficiencies in the IRI continue to be its representation of high-latitude phenomenology and the specification of E- and F-region densities in a way that allows the accurate inclusion of the E/F region valleys as well as intermediate, descending, and transitional layers. Advances are now being made in those areas, and it can be expected that there will be improvements in the IRI, its representation of monthly-averaged ionospheric properties, and in its adaptability to a time-dependent description of dynamic events.

Acknowledgements. This work has been supported by the National Science Foundation (NSF) under Grant No. ATM-9102298. To NSF and to all participating countries and institutions, the SUNDIAL team extends its sincere thanks for dedicated support to this international endeavor.

References

- Abdu, M. A., B. M. Reddy, G. O. Walker, R. Hanbaba, J. H. A. Sobral, B. G. Fejer, R. F. Woodman, R. W. Schunk, and E. P. Szuszczewicz, Processes in the quiet and disturbed equatorial-low latitude ionosphere: SUNDIAL campaign 1984, *Ann. Geophysicae*, **8**, 69–80, 1988.
- Abdu, M. A., G. O. Walker, B. M. Reddy, J. H. A. Sobral, B. G. Fejer, T. Kikuchi, N. B. Trivedi, and E. P. Szuszczewicz, Electric field versus neutral wind control of the equatorial anomaly under quiet and disturbed conditions: a global perspective from SUNDIAL 86, *Ann. Geophysicae*, **8**, 419–430, 1990.
- Abdu, M. A., G. O. Walker, B. M. Reddy, E. R. de Paula, J. H. A. Sobral, B. G. Fejer and E. P. Szuszczewicz, Global scale equatorial ionization anomaly (EIA) response to magnetospheric disturbances based on the May-June 1987 SUNDIAL coordinated observations, *Ann. Geophysicae*, (1993 in press).
- Bilitza, D., Electron density in the equinoctial topside, *Adv. Space Res.*, **5**, 15–19, 1985.
- Biondi, M. A., J. W. Meriwether, Jr., Y. Sahai, and H. Takahasni, Thermospheric neutral winds at low latitudes during the September-October 1986 SUNDIAL campaign: optical interferometer results, *Ann. Geophysicae*, **8**, 409–418, 1990.
- Denisenko, P. F., N. A. Zabolotn, D. S. Bratsun, and S. A. Pulnits, Detection and mapping of small-scale irregularities by topside sounding data, *Ann. Geophysicae*, (1993 in press).
- Evans, D. S., T. J. Fuller-Rowell, S. Maeda, and J. Foster, Specification of the heat input to the thermosphere from magnetospheric processes using NOAA TIROS auroral particle observations, *Adv. Astron. Sci.*, **65**, 1649, 1988.
- Emery, B. A., A. D. Richmond, H. W. Kroehl, C. D. Wells, J. M. Ruohoniemi, M. Lester, D. J. Knipp, R. J. Rich, J. C. Foster, O. dela Beaujardiere, C. Senior, L. M. Shier, J. F. McKee, and S. Maeda, Electric potential patterns deduced for the SUNDIAL period of September 23–26, 1986, *Ann. Geophysicae*, **8**, 399–408, 1990.
- Fejer, B. G., R. W. Spiro, R. A. Wolf, and J. C. Foster, Latitudinal variation of perturbation electric fields during magnetically disturbed periods: 1986 SUNDIAL observations and model results, *Ann. Geophysicae*, **8**, 441–454, 1990.
- Fuller-Rowell, T. J., and D. S. Evans, Height-integrated Pedersen and Hall conductivity patterns inferred from the NOAA TIROS satellite data, *J. Geophys. Res.*, **92**, 7606, 1987.
- Feldstein, Y. I., On morphology of auroral and magnetic disturbances at high latitudes, *Geomagn. Aeron.*, **3**, 183, 1963.
- Foster, J. C., J. M. Holt, R. G. Musgrove, and D. S. Evans, Ionospheric convection associated with discrete levels of particle precipitation, *Geophys. Res. Lett.*, **13**, 656–659, 1986.
- Hardy, D. A., M. S. Gussenhoven, R. Raistrick, and W. J. McNeil, Statistical and functional representation of the pattern of auroral energy flux, number flux, and conductivity, *J. Geophys. Res.*, **92**, 12275–12294, 1987.
- Holzworth, R. H. and C. I. Meng, Mathematical representation of the auroral oval, *Geophys. Res. Lett.*, **2**, 337–380, 1975.
- Kikuchi, T., H. Yamagishi, and M. Lester, Drift of auroral absorption due to the magnetospheric convection observed with the scanning narrow beam riometer during SUNDIAL '86, *Ann. Geophysicae*, **8**, 431–440, 1990.
- Leitinger, R., P. Wilkinson, and R. Hanbaba, The ionosphere in mid-latitudes during the SUNDIAL campaign, *Ann. Geophysicae*, **6**, 59–68, 1988.
- Lester, M., O. dela Beaujardiere, J. C. Foster, M. P. Freeman, H. Luhr, J. M. Ruohoniemi, and W. Swider, The response of the large scale ionospheric convection pattern to changes in the IMF and substorms: results from the SUNDIAL 1987 campaign, *Ann. Geophysicae*, (1993, in press).
- Miller, K. L., P. G. Richards, and H. Y. Wu, A global-scale study of meridional winds and electron densities in the F-region during the SUNDIAL '87 campaign, *Ann. Geophysicae*, (1993, in press).
- Rawer, K., *International reference ionosphere-IRI 79*, NOAA Rep., UAG-82, U.S. Dept. of Commerce, Washington, DC, 1981.
- Rawer, K. and Y. V. Ramanamurty, *International reference ionosphere-status 1985.86*, URSI COSPAR Workshop Proceedings, Belgium 28 October 1985, Wheaton & Co. Ltd., U.K., 1985.
- Richmond, A. D. and Y. Kamide, Mapping electrodynamic features of the high-latitude ionosphere from localized observations: technique, *J. Geophys. Res.*, **93**, 5741–5759, 1988.
- Robinson, R. M., R. R. Vondrak, K. Miller, T. Dabbs, and D. Hardy, On calculating ionospheric conductances from the flux and energy of precipitating electrons, *J. Geophys. Res.*, **92**, 2565–2569, 1987.

- Ruhoniemi, G. M., R. A. Greenwald, O. dela Beaugardiere, and M. Lester.** The response of the high-latitude dayside ionosphere on an abrupt northward transition in the IMF. *Ann. Geophysicae*, (1993, in press).
- Schunk, R. W. and E. P. Szuszczewicz.** First-principle and empirical modeling of the global-scale ionosphere. *Ann. Geophysicae*, **6**, 19-30, 1988.
- Sica, R., R. W. Schunk, and P. Wilkinson.** A study of the undisturbed mid-latitude ionosphere using simultaneous multiple-site ionosonde measurements during the SUNDIAL-86 campaign. *J. Geophys. Res.*, **95**, 8271-8279, 1990.
- Spiro, R. W., R. A. Wolf, and B. G. Fejer.** Penetration of high-latitude electric field effects to low latitudes during SUNDIAL 1984. *Ann. Geophysicae*, **6**, 39-50, 1988.
- Szczuszczewicz, E. P., B. Fejer, E. Roelof, R. Schunk, R. Wolf, R. Leitinger, M. Abdu, B. M. Reddy, J. Joselyn, P. Wilkinson, and R. Woodman.** SUNDIAL: a worldwide study of interactive ionospheric processes and their roles in the transfer of energy and mass in the Sun-Earth system. *Ann. Geophysicae*, **6**, 3-18, 1988.
- Szczuszczewicz, E. P., P. Wilkinson, M. A. Abdu, E. Roelof, R. Hanbaba, M. Sands, T. Kikuchi, R. Burnside, J. Joselyn, M. Lester, R. Leitinger, G. O. Walker, B. M. Reddy, and J. Sobral.** Solar-terrestrial conditions during SUNDIAL-86 and empirical modeling of the global-scale ionospheric responses. *Ann. Geophysicae*, **8**, 387-390, 1990.
- Szczuszczewicz, E. P., B. Fejer, E. Roelof, R. Schunk, R. Wolf, M. Abdu, T. Bateman, P. Blanchard, B. A. Emery, A. Feldstein, R. Hanbaba, J. Joselyn, T. Kikuchi, R. Leitinger, M. Lester, J. Sobral, B. M. Reddy, A. D. Richmond, R. Sica, G. O. Walker, and P. Wilkinson.** Modelling and measurement of global-scale ionospheric behavior under solar minimum, equinoctial conditions. *Adv. Space Res.*, **12**, 105-115, 1992.
- Walker, G. O., T. Y. Y. Li, J. Soegijo, T. Kikuchi, Y. N. Huand, V. Badillo, and E. P. Szuszczewicz.** North-South asymmetry of the equatorial anomaly observed in East Asia during the SUNDIAL-87 Campaign. *Ann. Geophysicae*, **9**, 393-400, 1991.
- Wilkinson, P. J. R. Schunk, R. Hanbaba, and H. Mori.** Interhemispheric comparison of SUNDIAL F-region data with global scale ionospheric models. *Ann. Geophysicae*, **6**, 31-38, 1988.
- Wilkinson, P. J., E. P. Szuszczewicz, and R. G. Roble.** Measurement and modelling of intermediate, descending, and sporadic layers in the lower ionosphere: results and implications for global-scale ionospheric-thermospheric studies. *Geophys. Res. Lett.*, **19**, 95-98, 1992.

Accession For		
NTIS	CRA&I	<input checked="" type="checkbox"/>
DTIC	DAE	<input type="checkbox"/>
Unannounced		<input type="checkbox"/>
Justification		
By _____		
Distribution _____		
Availability Codes		
Dist	Avail and/or Special	
A-1 20		

DTIC QUALITY INSPECTED 3